ACS APPLIED MATERIALS & INTERFACES

www.acsami.org

Research Article

Facile Post-deposition Annealing of Graphene Ink Enables Ultrasensitive Electrochemical Detection of Dopamine

Derrick Butler, David Moore, Nicholas R. Glavin, Joshua A. Robinson, and Aida Ebrahimi*

Cite This: *ACS Appl. Mater. Interfaces* 2021, 13, 11185−11194

Read Online

ACCESS | Metrics & More | Article Recommendations | Supporting Information

ABSTRACT: A growing body of research focuses on engineering materials for electrochemical detection of dopamine (DA), a critical neurotransmitter involved in motor function, reward processes, and blood pressure regulation. Among various sensing materials, graphene is highly attractive due to its excellent electrical conductivity and, in particular, the $\pi-\pi$ interaction between the aromatic rings of DA and graphene. However, the lowest detection limits reported solely using graphene are nominally 1 nM. To improve the sensor sensitivity, various strategies are being explored, including chemical functionalization, heterostructure/composite formation, elemental doping, and modification with biomolecules (aptamers, enzymes, *etc.*). In this work, we demonstrate that commercially available graphene ink can exhibit selective and highly sensitive detection of DA by tuning the surface chemistry utilizing a simple, one-step annealing process. The annealing condition directly impacts the sensor response to DA, with the optimal conditions (30 min at 300 °C under 3% H_2 + Ar) yielding a distinguishable and selective response to DA down to 5 pM. X-ray photoelectron spectroscopy (XPS) confirms that the improved selectivity is due to the increased fraction of oxygen functionalities (in particular, C−OH), while Raman spectroscopy shows a higher degree of defectiveness for this condition compared to others. Evaluation of the interaction of three molecular components of DA (*i.e.*, aromatic ring, hydroxyl groups, and amine group) with graphene confirms that the $\pi-\pi$ interaction and −OH groups play a prominent role in the improved adsorption of DA on the graphene surface. Furthermore, we demonstrate a proof-of-concept, all-solution processable sensor on polyimide substrates using graphene ink. Tuning the sensor response by varying the annealing condition offers a simple avenue for developing sensitive, selective, and low-cost point-of-care biosensors, while low-temperature annealing ensures compatibility with flexible substrates, such as polyimide.

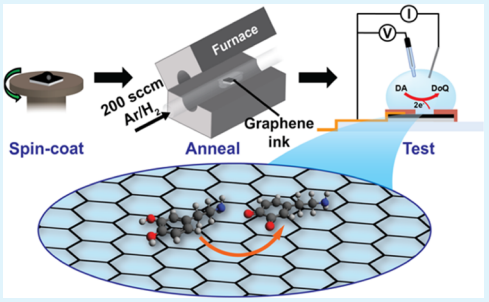

KEYWORDS: *graphene ink, surface chemistry, annealing, dopamine, electrochemical sensor, biosensor, ethyl cellulose, scanning electrochemical microscopy*

INTRODUCTION

Dopamine (DA, 3-hydroxytyramine) is a critical catecholamine and neurotransmitter found in the human brain and kidney.[1,2] This molecule is a requisite in physiological processes such as motor function, emotions, reward processes, and blood pressure regulation.[1,2] DA also serves as a precursor for *in vivo* synthesis of other catecholamines, such as epinephrine and norepinephrine.[3] Importantly, deviations from normal, healthy levels of DA in blood plasma (~740 pM)[4] can be symptomatic of Parkinson's disease, Alzheimer's disease, schizophrenia, and hypertension.[2,5] Current clinical techniques for monitoring DA levels include traditional blood tests and 24 h urine sampling.[6] These tests, although effective, rely on trained technicians with advanced laboratory instrumentation, such as liquid chromatography, and may prove difficult for point-of-care (PoC) applications.[7,8]

Electrochemical sensors are exceedingly attractive for detection of DA considering its high redox-activity.[9] Furthermore, electrochemical sensors are becoming a preferred means for PoC detection of numerous bioanalytes, in part due to real-time readout, simple testing schemes, low-cost, scalable manufacturing, and compatibility with the integrated circuit technology for data acquisition, processing, and transfer.[7,10,11] Electrochemical techniques rely on detecting the oxidation of DA to dopamine-*o*-quinone.[10] Among the multitude of electrochemical methods, differential pulse voltammetry (DPV) enables sensitive detection of a target species by overlaying periodic pulses on top of a continuous linear potential sweep.[12] These pulses serve to reduce the non-faradaic component of the current and exemplify the faradaic component, which is of analytical interest.[12] Thus, DPV provides sensitive detection of various redox-active analytes, such as DA, for example, down to 24 nM in the presence of ascorbic acid (AA).[10] In another work, Khudaish et al.

Received: November 30, 2020
Accepted: January 13, 2021
Published: February 27, 2021

https://dx.doi.org/10.1021/acsami.0c21302
ACS Appl. Mater. Interfaces 2021, 13, 11185−11194

demonstrated a glassy carbon electrode modified with poly-(2,4,6-triaminopyrimidine) and Au nanoparticles to detect down to 17 nM of DA in the presence of both uric acid (UA) and AA, two common interfering species.[13]

Following its isolation in 2004,[14] graphene, a two-dimensional (2D) honeycomb-like lattice of carbon atoms, has been extensively studied for applications ranging from field-effect transistors and circuits,[15] to solar cells,[16] protective coatings,[17] and targeted therapeutics,[18] among others. Additionally, graphene and its derivatives are frequently utilized in electrochemical biosensors, both as an active sensing layer and as a conductive substrate to support other nanomaterials.[19−21] Graphene is a viable sensing material for DA detection due to the $\pi-\pi$ interaction between the aromatic rings of DA and graphene.[22] Moreover, favorable electrostatic interactions between graphene (often negatively charged at neutral pH)[23] and DA (positively charged at neutral pH ($pK_a = 8.87$)) make it a suitable sensor for dopamine. Functionalizing graphene and its derivatives with metal or metal oxide nanoparticles,[7] dopants,[21] or conductive polymers[24] can further enhance the electrochemical response to DA. The use of graphene inks—colloidal suspensions of graphene flakes—provides an additional morphological advantage in that the porous nature of the deposited film can improve the electrochemical response by modulating the mass transport.[25]

Thus far, aptasensors (sensors based on aptamers—oligonucleotides or peptides that bind to the desired target analyte) provide the lowest DA detection limits, a crucial figure of merit for biosensors. Wang et al. demonstrated a highly responsive aptasensor based on a reduced graphene oxide (rGO)/poly(3,4-ethylenedioxythiphene) composite for detecting as little as 78 fM of DA.[26] Another aptasensor from Liu et al. utilized graphene and polyaniline for sensitive detection of DA down to 1.98 pM.[27] Although they display remarkable sensing properties, aptasensors can still suffer from high functionalization costs and complexities, as well as environmental instabilities.[28] On the contrary, DA sensors based solely on graphene leverage its scalability and low manufacturing costs.[29] For example, Yang et al. demonstrated electrochemically reduced graphene oxide without further modification for detection of DA down to 500 nM.[30] However, if electrochemical sensors based on graphene are to become an effective means for DA detection, analytical operation in the range of 100's of pM to low nM is necessary.

One such approach for the scalable production of graphene is through the controlled ablation of a polymer using a CO_2 laser.[31] Termed "laser-induced graphene (LIG)," this approach allows for maskless, direct patterning of conductive and highly porous graphene structures without the need for high-temperature growth or wet chemical processes.[32] This technique has been demonstrated in the development of electrochemical sensors[33−36] and shows great potential for developing low-cost sensing platforms for DA. One possible drawback is that the choice of the substrate is limited to polymers, such as polyimide, and other carbonaceous materials. The use of graphene ink, on the other hand, allows for deposition on potentially any solid substrate. Therefore, LIG and graphene ink are complementary means that hold remarkable viability for the development of low-cost biosensing platforms.

Herein, we report a facile and scalable post-deposition annealing process to tune the surface chemistry of commercial graphene ink without the need for subsequent chemical or biomolecular functionalization. Heat treatment has previously been used to tune the electrochemical response of graphene sensors.[37] Building upon our preliminary studies with graphene ink-based electrochemical sensors,[38] we achieve a highly sensitive and selective electrochemical response to DA down to 5 pM, the lowest reported among existing graphene-only electrochemical DA sensors. The effect of the annealing condition is examined as a means to tune the graphene−DA interaction and identify the optimal condition for DA detection—30 min at 300 °C under 3% H_2 + Ar. We find that a larger concentration of oxygen functionalities (in particular, C−OH) correlates with a higher sensitivity to DA. These findings are confirmed by studying three possible adsorption mechanisms using DA, phenylethylamine (PEA; contains an amine group and an aromatic ring), and propylamine (PA; contains only an amine group)[39] and are in good agreement with previous studies.[40,41] Additionally, in order to translate the graphene ink sensor toward a portable PoC platform, we demonstrate a flexible, all-solution processable sensor based on patterned graphene ink without the need for using microfabrication processes.

EXPERIMENTAL SECTION

Materials. Graphene ink optimized for spray/spin-coating (cat. # 900960, Millipore-Sigma; St. Louis, MO, USA) was used without modification unless otherwise stated. (3-mercaptopropyl) trimethoxysilane (MPTS), toluene (anhydrous, 99.8%), potassium hexacyanoferrate(II), potassium hexacyanoferrate(III), DA hydrochloride, AA, and UA were all purchased from Millipore-Sigma (St. Louis, MO, USA). Ethanol (Koptec, 200 proof) was purchased from Decon Labs (King of Prussia, PA, USA). Isopropyl alcohol (99.5%, SemiGrade) and acetone (99.5%, SemiGrade) were purchased from VWR (Radnor, PA, USA). Phosphate-buffered saline (PBS, 1×, pH 7.4) and fetal bovine serum (U.S. origin, no heat inactivation) were purchased from Corning (Corning, NY, USA). Conductive silver epoxy was purchased from MG Chemicals (Burlington, ON, Canada) and prepared by combining equal parts of the precursors and thoroughly mixing. Polyimide sheets (Kapton GS 500) were obtained from DuPont Inc. (Wilmington, DE, USA).

Processing of the Graphene Ink. The graphene ink sensor was fabricated on silicon-on-insulator (SOI) wafers. The wafers were first cut into 1 × 1 cm^2 pieces and cleaned through sequential ultrasonication in acetone and isopropanol for 10 min each, rinsed in deionized (DI) water (Milli-Q, 18.2 MΩ cm at 25 °C), and dried with N_2. After cleaning, the substrates were immersed overnight (~15 h) in an MPTS solution (5% by vol. in toluene) to promote film adhesion and uniformity. The substrates were rinsed with toluene and dried before spin-coating (Laurell Technologies WS-650MZ). Next, 50 μL of the graphene ink was spin-coated onto the substrate. For samples prepared with diluted ink, the ink was diluted 1:2 by volume with ethanol and vortexed to ensure uniform mixing. After spin-coating, the sensors were annealed either on a hot plate (pre-heated to desired temperature) or in a tube furnace (Barnstead-Thermolyne F21135). For samples annealed in the furnace under (0%, 3%, or 15%) H_2 + Ar gas mixture, a flow rate of 200 sccm and a pressure of 700 Torr were used. The heating rate was 50 °C/min.

Material Characterization. Scanning electron microscopy (SEM) images were taken with a FEI NanoSEM 630 microscope (Hillsboro, OR, USA). The samples were coated with ~5 nm of iridium prior to imaging. Atomic force microscopy (AFM) measurements were taken using a Bruker Icon instrument (Santa Barbara, CA, USA). NanoScope Analysis 1.9 was used to calculate film roughness and thickness after first-order flattening of the AFM images. Film thickness measurements were performed after spin-coating by removing a portion of the film using a cotton swap and isopropanol. The step height between the substrate and the film was taken as the film thickness.

X-ray photoelectron spectroscopy (XPS) measurements were conducted in a Physical Electronics VersaProbe II instrument

https://dx.doi.org/10.1021/acsami.0c21302
ACS Appl. Mater. Interfaces 2021, 13, 11185−11194

(Chanhassen, MN, USA). An Al Kα X-ray source (1.49 keV) was used, and charge neutralization was carried out using low energy (<5 eV) electrons and Ar ions. Charge calibration was performed using the sp^2 carbon peak at 284.4 eV.[42] Measurements were made at a takeoff angle of 45° with respect to the sample. A pass energy of 23.5 eV was used. Spectra were analyzed using CasaXPS software with the appropriate instrumental relative sensitivity factors. A Tougaard background was used for all spectra. An sp^2 C1s line shape was obtained from highly ordered pyrolytic graphite measured on the same equipment, in order to better account for the inherent asymmetry of this peak in the fitting of the graphene ink spectra.[42]

Raman spectroscopy was conducted using a Horiba LabRam instrument (Kyoto, Japan) with a 100× objective and 1800 g/mm grating. A 532 nm (2.33 eV) laser with a max power of 110 mW operating at 5% power was used. Spectra were analyzed using the LabSpec 6 software. The background was subtracted using a second-order fit before calculating the peak intensity ratios. The peaks were fit with combined Gaussian−Lorentzian curves. The peak intensity ratios were calculated based on the fitted peak amplitudes.

Sheet Resistance Measurements. Sheet resistance measurements were performed in a Cascade 1200 four-point probe station. Indium dots were pressed into each corner of the sample in a van der Pauw configuration. The samples were then annealed at 180 °C for 1 min on a hot plate. I−V measurements were initially carried out to ensure that an ohmic contact was formed before carrying out the van der Pauw sheet resistance measurements. More details are provided in the Supporting Information.

Sensor Assembly and Electrochemical Characterization. Polyimide tape was used to isolate the active sensing area using a 2 mm diameter biopsy punch. Electrical contact was made with adhesive copper tape. Electrochemical characterization was carried out using a three-electrode configuration with a Pt wire as the counter electrode (CE) and Ag/AgCl (saturated in 3 M NaCl) as the reference electrode (RE). All results here are referenced to this RE, unless otherwise noted. The measurements were taken using a PalmSens4 potentiostat (BASi Co., Lafayette, IN, USA) with the PSTrace 5 software. For electrochemical testing, 100 μL of solution was pipetted onto the sensor.

For DPV measurements, a pulse amplitude of 200 mV, pulse duration of 20 ms, and scan rate of 50 mV s^{-1} were used. Before measurement with DA, the graphene sensors are stabilized *via* multiple (~10) CV scans in PBS from −0.6 to 0.6 V. Once stabilized, DA concentrations from 0 pM to 50 μM in PBS are tested with each graphene electrode using DPV. The baseline of the DPV curves was subtracted using a spline fit by selecting points along the curve both preceding and proceeding the potential range corresponding to the faradaic peak and interpolating the fitted curve through these points.[43] This processing was performed in OriginLab's OriginPro 2019 software.

Electrochemical impedance spectroscopy (EIS) measurements were carried out with 5 mM $[Fe(CN)_6]^{3-/4-}$ in PBS across a frequency range of 100 mHz to 1 MHz. An AC potential of 10 mV was applied with a DC potential of 0 V with respect to the open-circuit potential. A Randles equivalent circuit model with two resistor−capacitor (RC) components was used to extract the charge transfer and intrinsic resistance values. The circuit fitting was performed using the EIS Spectrum Analyzer software. Cyclic voltammetry (CV) measurements with $[Fe(CN)_6]^{3-/4-}$ were carried out at a scan rate of 50 mV s^{-1}. The faradaic component of the CV curves was calculated by linearly extrapolating the non-faradaic component and subtracting its contribution from the faradaic peak.

The error bars reported for the electrochemical measurements represent the standard error (SE) of the mean and were calculated from the testing of four to five distinct sensors (n = 4−5) for each processing condition.

Scanning Electrochemical Microscopy Characterization. Scanning electrochemical microscopy (SECM) measurements were carried out on a Bruker Dimension Icon AFM system with Bruker PeakForce SECM probes (Santa Barbara, CA, USA). The solution was 1 or 100 mM DA hydrochloride in PBS. The measurement was carried out in a four-electrode chamber with Pt wire CE, Ag/AgCl RE, and the probe tip and sample surface as the two WEs. Initial CV curves with the tip and surface separated by 1 mm distance were used to ensure connectivity and to find the equilibrium potential. The probe tip was then held 150 mV above the equilibrium potential and the surface 150 mV below. Various other potentials were applied for repeatability. A map of the tip current was taken with an interleave lift scan. That is, the topography was measured by the standard liquid phase tapping mode and then the probe was lifted 20 nm and retraced the measured topography. Lift heights of 50 nm and 250 nm were also employed.

Fabrication of an All-Solution Processable Sensor Based on Graphene. The all-solution processable sensor based on graphene ink was fabricated on a polyimide sheet (5 mil thick, DuPont Inc., Wilmington, DE, USA) cleaned *via* sequential ultrasonication in acetone and isopropanol for 10 min each, rinsed in DI water, and dried with N_2. A sacrificial mask layer of the polyimide tape was applied on the sheet and patterned with a CO_2 laser printer (λ = 10.6 μm; VLS 2.30 Desktop Laser System, Universal Laser Systems Inc., Scottsdale, AZ, USA) operating in the vector mode at 7.5 W power (30% of max), 1000 pulses per inch, and a write speed of 2.9 in. per second (29% of max). AutoCAD (AutoDesk, San Rafael, CA, USA) was used to create the pattern. The patterned regions were removed, and two layers of graphene ink were spin-coated at 2000 rpm for 30 s, followed by annealing for 30 min at 300 °C under 3% H_2 + Ar. The Ag/AgCl pseudo-reference electrode (PRE) was formed by depositing conductive silver epoxy onto the ink and curing for 2 h at 65 °C in an oven and treating with a 10:1 dilution of bleach in DI water for 1 min.

RESULTS AND DISCUSSION

Processing and Morphological Characterization of Graphene Ink Films. The fabrication and electrochemical testing scheme of the sensors based on graphene ink thin films is presented in Figure 1a. First, the effect of spin rate (2000 *vs* 5000

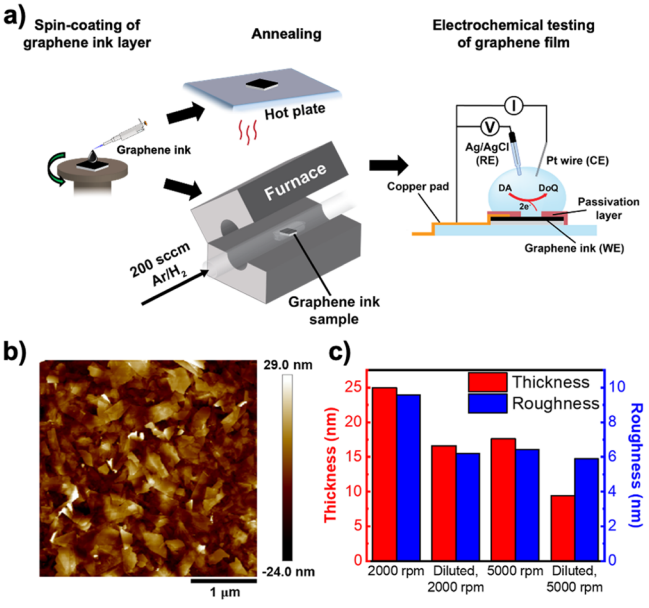

Figure 1. (a) Schematic outlining the fabrication and electrochemical testing process of the graphene ink DA sensor. The effects of the spin-coating and annealing conditions on the sensor performance are investigated. A three-electrode electrochemical cell comprising the graphene working electrode (WE), Pt wire counter electrode (CE), and Ag/AgCl reference electrode (RE) is used. (b) Representative AFM image showing a film of graphene flakes deposited on the substrate. (c) Film thickness and average roughness (R_a) of the as-received and diluted (1:2 by vol.) ink deposited at 2000 and 5000 rpm, as determined by AFM.

https://dx.doi.org/10.1021/acsami.0c21302
ACS Appl. Mater. Interfaces 2021, 13, 11185−11194

rpm) and ink dilution (as-received *vs* 1:2 volume dilution) on the surface morphology, sheet resistance, and charge transfer characteristics is investigated. More details can be found in the Supporting Information. Briefly, AFM is used to quantify film roughness (R_a) and thickness (Figure 1b,c). A roughness value of approximately 6 nm is measured for all conditions excluding the as-received ink spun at 2000 rpm ($R_a \sim 9.2$ nm). Higher roughness can be advantageous for electrochemistry as there is more active surface available within a given geometric area. Indeed, electrochemical characterization (Figure S1) with a ferri/ferrocyanide ($[Fe(CN)_6]^{3-/4-}$; 5 mM in PBS) redox probe shows more ideal charge transfer behavior for the as-received ink, with the 5000 rpm sample displaying the lowest charge transfer resistance and better sample-to-sample consistency. Furthermore, the sheet resistance (R_{sheet}) for graphene films using the as-received ink is lower than their diluted counterparts (Figure S1f). In combination, these improved electrical and electrochemical characteristics, in general, lead to improved sensing behavior. Thus, the as-received ink spun at 5000 rpm is chosen as the optimal deposition condition for the fabrication of DA sensors.

After spin-coating, the samples are thermally annealed to decompose the ethyl cellulose stabilizing polymer and remove residual solvent, thereby significantly enhancing the electrical conductivity which is necessary for electrochemical sensing applications.[44] Other techniques, such as photonic annealing[44] and pulsed-laser-annealing (PLA),[45,46] have also been shown to improve the electrical conductivity of graphene ink films. These techniques use high-energy light to decompose the ethyl cellulose binder and increase conductivity. An advantage of such strategies is the compatibility with substrates and auxiliary processing materials that cannot withstand thermal annealing. However,photonic annealing and PLA modalities result in film morphologies that differ from thermally annealed samples.[44−46] These morphologies have been exploited, for example, to create superhydrophobic surfaces,[46,47] due to the vertical alignment of graphene flakes compared to horizontally aligned flakes after casting and thermal annealing. Additionally, these techniques can mitigate and remove oxygen functionalities from the surface (which generally increase hydrophilicity).[44−47] Although the resulting graphene may be suitable for applications in anti-fouling and self-cleaning surfaces, it may not be ideal for sensing applications. Good surface wetting is desirable for electrochemical sensing as it allows for more facile diffusion of the analytes to the electrode surface.[48,49] Furthermore, the presence of oxygen moieties on the surface can enhance the interaction with a target analyte, which subsequently improves the sensor performance.[50,51] As a result, thermal annealing is chosen here because of better hydrophilicity and a higher degree of oxidation. However, despite the drawbacks listed here, photonic annealing does have its advantages and has even been used recently for applications in biosensing.[52]

We investigate the effect of annealing temperature, duration, and environment on the sensor performance. The annealing temperature and duration impact the resistivity of graphene ink electrodes,[44−46] whereas the underlying mechanism of ethyl cellulose decomposition is dependent on the annealing environment.[53] To this end, four different annealing conditions (outlined in Table 1) are evaluated to understand the role of annealing time (30 min *vs* 180 min), temperature (300 *vs* 1000 °C), and environment (on a hot plate or in a tube furnace under 3% H_2 + Ar) in the sensing response to DA. Our studies on the effect of H_2 content show that 3% H_2 yields the largest DA

Table 1. Annealing Conditions of the Graphene Ink Studied in this Work

	Graphene annealing conditions		
Sample identifier	Time (min)	Temperature (°C)	Environment
S_{1000}	30	1000	3% H_2 + Ar
$S_{300,30}$	30	300	3% H_2 + Ar
S_{HP}	30	300	hot plate
$S_{300,180}$	180	300	3% H_2 + Ar

oxidation peak current (see Figure S2). The pyrolysis of ethyl cellulose occurs at approximately 300 °C;[53] hence, this temperature is chosen for investigation as it is possible to decompose the ethyl cellulose without completely removing the byproducts. Lower temperatures would result in incomplete decomposition of the ethyl cellulose resulting in poor electrical properties.[44] Conversely, at 1000 °C, all residual polymer or solvent will be removed.[54] Additionally, 30 min has been reported to be sufficient for obtaining highly conductive graphene ink films,[54] but longer times are less explored. Therefore, a longer annealing time of 180 min is also chosen for investigation.

Studying the Interfacial Properties and Charge Transfer of Graphene Ink Layers. The electrochemical properties of the ink-based working electrodes (WEs) are evaluated using CV and EIS measurements with a $[Fe(CN)_6]^{3-/4-}$ redox probe. $[Fe(CN)_6]^{3-/4-}$ electron transfer is surface sensitive, although not oxide sensitive, meaning that the electron transfer is slowed by the presence of surface monolayers and not dependent on the specific type of oxygen-containing functional groups.[55]

CV (Figure 2a) provides insights into the electrode kinetics and reversibility,[12] where a ~57 mV peak separation (ΔE_{peak}) (for single electron transfer reaction at 25 °C) indicates ideal reversibility. Divergence from this ideal value corresponds to more sluggish electron transfer kinetics and worsened reaction

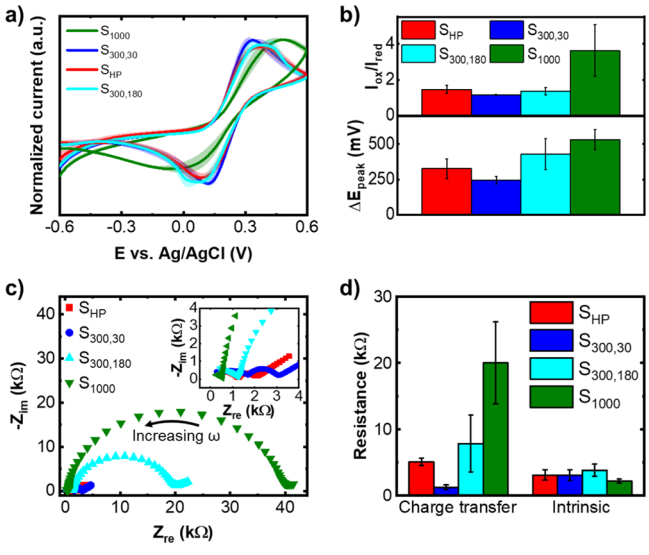

Figure 2. Electrochemical characterization of graphene films using CV and EIS methods with 5 mM $[Fe(CN)_6]^{3-/4-}$ in PBS (pH = 7.4). (a) Average normalized CV data for each annealing condition. The shaded region represents the SE of 4−5 samples. Representative cyclic voltammograms of each processing condition with (b) relevant kinetic parameters shown. (c) Nyquist plots for each processing condition, with the high-frequency region shown in the inset. (d) Extracted charge transfer and intrinsic resistance values for each processing condition.

https://dx.doi.org/10.1021/acsami.0c21302
ACS Appl. Mater. Interfaces 2021, 13, 11185−11194

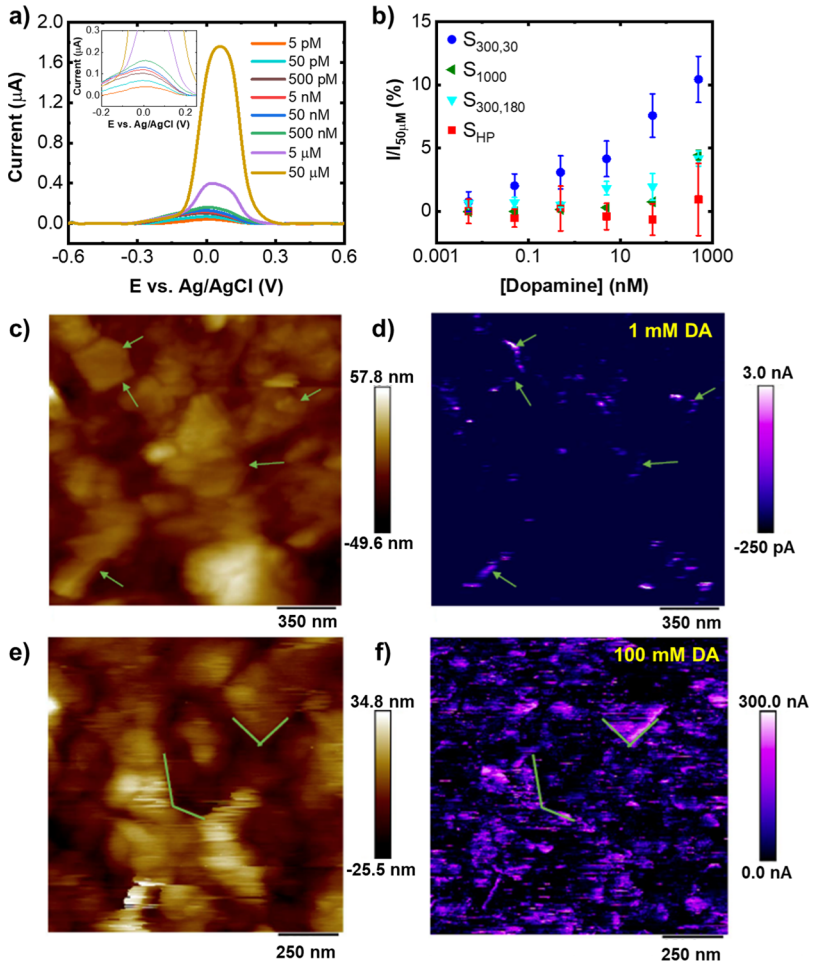

Figure 3. (a) A representative differential pulse voltammogram of $S_{300,30}$ (the optimal condition for DA detection) after background subtraction. The inset shows the response at lower DA concentrations. (b) Normalized peak current values versus DA concentration for each annealing condition (n = 4−5). (c) A height map measured using SECM and (d) the corresponding electrochemical map with 1 mM DA. (e) A height map of a different region of the graphene film and (f) the corresponding electrochemical map with 100 mM DA. Note—the arrows and lines serve to guide the eyes when comparing between the height maps and corresponding electrochemical maps.

reversibility. Figure 2a shows the normalized CV curves for each annealing condition, with the shaded region representing the standard error of 4−5 samples. The graphene ink annealed at 300 °C for 30 min in 3% H_2 + Ar ($S_{300,30}$) exhibits a peak separation of 245 ± 27 mV, the lowest of the four conditions investigated (Figure 2b). Similar values have been reported for screen-printed graphene ink electrodes.[56] This condition also exhibits the lowest faradaic peak current ratio (I_{ox}/I_{red} = 1.15 ± 0.05, ideally unity), an additional figure of merit describing the reversibility of an electron transfer process.[12] On the contrary, samples annealed at 1000 °C for 30 min in 3% H_2 + Ar (S_{1000}) demonstrate the worst performance, with a ΔE_{peak} of 533 ± 72 mV and a I_{ox}/I_{red} of 3.62 ± 1.44. High-temperature annealing in the presence of hydrogen is known to restore sp^2 domains, remove oxygen-containing functional groups, and passivate the electrochemically active edge sites.[57] This likely explains the poor electrochemical performance of S_{1000} as defects play an important role in improving the electrochemical activity. Furthermore, we observe a significant decrease in the sheet resistance of S_{1000} (Figure S3), which is typical of less defective graphene and agrees well with previous reports.[46] The 300 °C, 180 min, ($S_{300,180}$) condition also shows slower electrochemical kinetics (ΔE_{peak} = 430 ± 109 mV, I_{ox}/I_{red} = 1.37 ± 0.21), suggesting the longer annealing duration, even at lower temperatures, may also reduce defectiveness.

EIS measurements further elucidate the interfacial properties of the graphene layer. The Nyquist plots (Figure 2c) are fitted with two RC circuits composed of a high-frequency semicircular region, a mid-frequency semicircular region, and a low-frequency linear region. The low-frequency linear region arises from mass transport limitations and is described by the Warburg impedance, Z_W.[12] The high-frequency semicircle corresponds to the intrinsic impedances of the material (*e.g.*, flake to flake, contact impedance)[58] and is denoted as R_{int}. The intrinsic resistance remains relatively constant at 2.5−3 kΩ across all conditions (Figure 2d). The mid-frequency semicircle is attributed to the faradaic charge transfer resistance, denoted as R_{ct}. R_{ct} varies dramatically across processing conditions and follows a similar trend to ΔE_{peak} extracted from the CV data (as shown in Figure 2b), in agreement with previous reports.[59,60] S_{1000} shows the largest charge transfer resistance with R_{ct} = 20.00 ± 6.20 kΩ, while $S_{300,30}$ exhibits the smallest R_{ct} (1.23 ± 0.35 kΩ). Therefore, we conclude that $S_{300,30}$ exhibits the most favorable electron transfer characteristics of the four conditions studied, which often correlates to improvements in electrochemical sensing applications.[61]

https://dx.doi.org/10.1021/acsami.0c21302
ACS Appl. Mater. Interfaces 2021, 13, 11185−11194

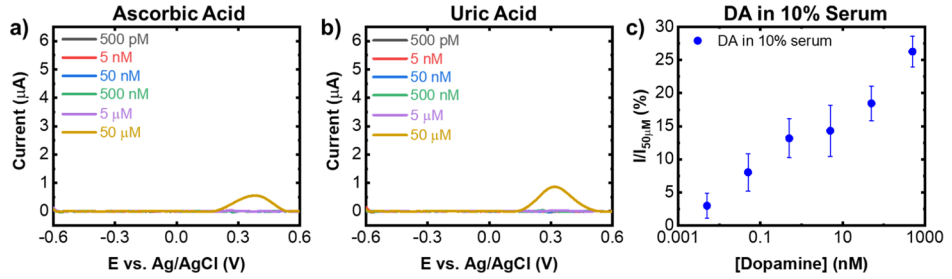

Figure 4. Graphene ink sensor is selective against (a) AA and (b) UA, which are two common interferents in detection of DA. No response is seen for either interferent below 50 μM. (c) Normalized DA response in a 10% serum solution (n = 3).

Tailoring the Sensor Response *via* the Annealing Condition. The effect of annealing on the graphene sensor response toward DA is investigated using DPV. An oxidation wave appears at ∼0 mV versus Ag/AgCl (Figure 3a). This peak corresponds to the oxidation of DA to dopamine-*o*-quinone *via* a two-electron transfer process.[7] Interestingly, the peak appears to be bimodal with two overlapping peaks present. Such behavior may be attributed to competing mass transport mechanisms, namely semi-infinite and thin-layer diffusion, related to the electrode morphology.[62−64] Oftentimes, thin-layer diffusion within the pores of the electrode gives rise to an oxidation peak shifted to more negative potentials relative to its semi-infinite counterpart. Given the spin-coated graphene films investigated here are much thinner (∼20 nm) than many of the drop-cast films studied by Aksay and co-workers (>1 μm),[63] the cumulative pore volume is less. Therefore, the predominant, although not exclusive, diffusive component is semi-infinite diffusion from the bulk solution. This is confirmed by the dependence of the redox peak current on the square root of the voltammetric scan rate (Figure S4), which is characteristic of semi-infinite planar diffusion described by the Randles−Ševčík equation.[12] Although the majority of mass transport in this case is due to semi-infinite diffusive transport, the additional element of electrode porosity may contribute to the improved DA response seen here. Expanding upon the role of film thickness and subsequent porosity in DA detection certainly warrants future investigation.

The normalized peak currents for each condition (after baseline subtraction (see Experimental Section), Figure 3b) as a function of DA concentration indicate that annealing in 3% H_2 + Ar at 300 °C for 30 min ($S_{300,30}$) is ideal, with a dynamic range of 5 orders of concentration magnitude (5 pM to 500 nM). Here, the current recorded at E = 0 mV versus Ag/AgCl for each concentration is normalized with respect to the current with 50 μM DA. S_{1000} and $S_{300,180}$ respond similarly to DA (detection limit ∼5 nM), while the sample annealed on a hot plate at 300 °C for 30 min (S_{HP}) exhibits the worst affinity to DA, with no significant response below 5 μM.

The enhanced response of $S_{300,30}$ to DA is partially attributed to the abundance of active edge plane sites of the graphene flakes. Edge plane sites have been reported to demonstrate heterogeneous electron transfer (HET) rates on the order of 10^{-2} cm s^{-1}, while the basal plane yields a HET rate below 10^{-9} cm s^{-1}, essentially inert.[66] Scanning electrochemical microscopy (SECM) allows for combined AFM height and electrochemical mapping, enabling direct visualization of physical features and their electrochemical behavior. The SECM tip current has two contributing factors: ambient current from the surrounding solution and enhanced current from the surface. When the tip is held above the redox potential of the solution and the surface is held below, or vice versa, the surface current dominates over an order of magnitude higher than the ambient tip current, which is mostly constant at a given lift height. Non-faradaic current and surface conductivity enhancement are determined to be negligible in controls. To ensure that this was not a measurement artifact from tip contact with the surface, both scan directions are observed. Similarly, lift heights of 20, 50, and 250 nm and several configurations of surface and probe potential all showed similar results.

We confirm the high electrochemical activity of edge sites using SECM mapping of the graphene layer (Figure 3c−f), which shows notably higher oxidation current at the edges of graphene flakes. Figure 3c,e show the height maps for two different regions of the graphene ink film. The arrows and lines serve as a guide for the reader and allow for easier comparison with the electrochemical maps, as shown in Figure 3d,f. Figure 3d shows the electrochemical mapping with 1 mM DA in PBS. The most active regions are located near the edges of individual flakes. This is especially clear for the flakes in the top and bottom left-hand corners of Figure 3d. Figure 3f shows the electrochemical mapping for a different region of the graphene film using 100 mM DA in PBS. At these concentrations, the overall activity is increased as seen by the increased magnitude of the current. Although the edge planes still show a significant electrochemical response, the basal planes begin to respond as well.

Analysis of the Raman spectra (Figure S5) of each annealing condition shows the presence of D (∼1350 cm^{-1}), D′ (∼1620 cm^{-1}), G (∼1580 cm^{-1}), and 2D (∼2700 cm^{-1}) peaks associated with graphitic carbon species.[67] The G peak arises from the degenerate longitudinal and in-plane transverse optical phonon modes at the Brillouin zone center (Γ) and is common for graphitic carbon.[67] The D peak is attributed to the in-plane transverse optical phonon mode at the *K*-point and arises due to defects and edges in graphene.[67] Comparison of the D and G peak intensities (denoted I_D and I_G, respectively) indicates moderate defectiveness ($I_D/I_G = 0.47 \pm 0.02$) for $S_{300,30}$, which is the most defective of the four conditions. On the contrary, the lowest I_D/I_G of 0.37, corresponding to S_{HP}, shows reduced performance in the detection of DA. The increased defectiveness explains, at least in part, the enhanced electrochemical performance. Defects in graphene have been shown to enhance electron transfer and improve the response to DA.[68] However, excessive defectiveness can degrade the electrical properties of graphene and worsen the sensing performance. Therefore, a modest degree of defectiveness, as seen here, allows for an improved electrochemical response (charge transfer with the solution) while maintaining much of the superlative electrical character of graphene (charge transport within the film).

https://dx.doi.org/10.1021/acsami.0c21302
ACS Appl. Mater. Interfaces 2021, 13, 11185−11194

Selectivity toward common interfering species is critical in biosensing technologies. In the case of DA, AA and UA are coexisiting species that can inhibit DA detection. To this end, we investigate the response of the optimal graphene ink layer ($S_{300,30}$) with both AA and UA using DPV. The results are shown in Figure 4a,b for AA and UA, respectively. As depicted, no significant response is observed at concentrations below 50 μM. Additionally, the oxidation potentials of both AA and UA occur at ~0.35 and ~0.30 V, respectively, whereas the DA oxidation peak occurs at ~0 V, thus limiting any overlap of the peaks. The selectivity of graphene films has been attributed to both its morphology[25] and the negative charge due to various oxygen-containing functional groups on the surface. Compared to DA with p$K_a \approx 8.9$, both AA and UA are negatively charged at physiological pH (with pK_a = 4.2 and 5.4, respectively),[69] leading to electrostatic repulsion from the graphene surface and improved selectivity for DA.

Furthermore, the sensor is capable of DA detection in a complex sample matrix - serum - as shown in Figure 4c. A 10% solution of fetal bovine serum in PBS is spiked with increasing DA concentrations. The analytical operation of the sensor remains comparable to the results obtained with DA in a 100% PBS solution, thus demonstrating the efficacy of the sensor to function in more complex, physiologically relevant samples.

Oxygen Functionalities Play a Key Role in DA Detection. XPS measurements of the carbon C 1s and oxygen O 1s are taken for each processing condition (XPS spectra and a detailed fitting are shown in Figure S6 of Supporting Information). The main peak corresponds to sp^2 carbon (284.4 eV) and is fitted with an asymmetric Gaussian–Lorentzian curve.[42] A smaller, symmetric peak for sp^3 carbon is found at 285 eV. Additional peaks attributed to different oxygen moieties (hydroxyl (C–OH; 285.7 eV), epoxide (C–O–C; 286.8 eV), carbonyl (C=O; 288.0 eV), and carboxyl (O–C=O; 289.1 eV)) on the graphene surface can be seen at higher binding energies, most likely a result of the pyrolysis of the ethyl cellulose. Finally, a broad π–π^* satellite peak around 291 eV is observed as well. A comparison of the atomic concentrations of each component is shown in Figure 5a. Given

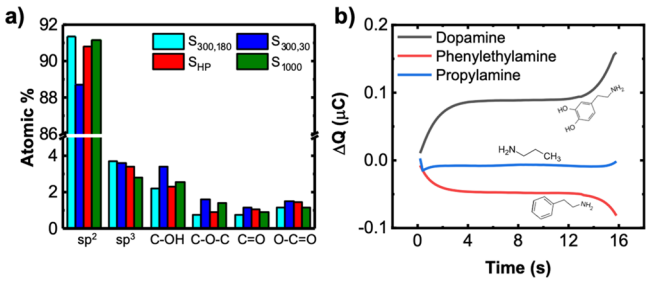

Figure 5. (a) Comparison of the atomic concentrations of each C 1s component based on fitting of the XPS spectra. (b) Three different amine-containing molecules (PA, PEA, and DA) are used to study adsorption on the surface (as indicated by $\Delta Q \equiv Q_{amine} - Q_{background}$) of graphene ink and confirm the XPS results.

the relatively low levels of oxygen-containing groups, the XPS data may only provide a semi-quantitative picture of the surface. Nonetheless, $S_{300,30}$ shows a higher level of hydroxyl groups than other conditions (around 3.75%). In fact, this condition shows higher levels of all oxygen functionalities. Recall that this condition yields the best electrochemical response to DA. The presence of hydroxyl groups in particular can lead to improved hydrogen bonding between graphene and DA and proves to be useful for sensing applications.[40] In tandem with other oxygen functionalities, the presence of hydroxyl groups on the surface likely contributes to the low-concentration DA response seen in the $S_{300,30}$ condition.

DA adsorption on graphene layers has been studied both experimentally[39,40] and computationally[41,70] to better understand how DA interacts with both pristine graphene and defective/functionalized graphene. DA adsorption is thought to occur through π–π interactions between the aromatic ring of the catechol group in DA and the carbon atoms of graphene, hydrogen bonding between –OH groups of DA and –OH groups on graphene, or dispersive interactions between charged groups (*e.g.*, amine, hydroxyl, and methylene) of DA and graphene.[40] In our work, the variation of surface chemistry as a function of annealing condition clearly impacts the electrochemical response to DA. Therefore, to better understand how graphene is interacting with DA, we employ a similar procedure previously reported by Bath et al.[39] Briefly, we test the non-faradaic interaction of graphene ink sensors with three different amine-containing molecules, namely DA, phenylethylamine (PEA), and propylamine (PA). Both PEA and PA lack specific molecular components found in DA that could act as adsorption sites. By limiting the potential scan window between –0.4 and 0 V, any faradaic processes will ideally be prevented, and therefore, the measured current is due to non-faradaic charge accumulation at the graphene–solution interface. Figure 5b shows the net charge (ΔQ; $\Delta Q \equiv Q_{amine} - Q_{background}$) as a function of time for each amine-containing species. Here, $Q_{background}$ and Q_{amine} represent the charge accumulated in the absence or presence of 5 μM of the target amine-containing molecule, respectively. For PA, which contains an amine group but no aromatic ring or hydroxyl groups, very little difference in charge can be seen between the background and 5 μM solution. This indicates that the amine group plays an insignificant role in adsorption of DA on the graphene surface. For PEA, an increase in the amount of negative charge accumulated for the 5 μM solution indicates that the aromatic ring increases adsorption on the surface through π–π interactions. This is consistent with computational studies, which have shown this interaction to be favorable.[41] The magnitude of ΔQ is largest for DA, thereby demonstrating the role of hydroxyl groups in DA adsorption on graphene as well. Hydroxyl groups are shown to form hydrogen bonds with hydroxyl groups and defects in graphene.[40,70] These defects may occur as vacancies in the basal plane[70] or along the edges of the graphene flake.[65] In this case, there appears to be less charge accumulated, as seen by the shift of the ΔQ to more positive values. This may be due to the presence of hydrogen bonds shifting the electron density from graphene to DA,[70] therefore resulting in less negative charge being present in the graphene layer. Thus, both hydroxyl groups and the π–π interaction are shown to play an important role in promoting DA adsorption on the graphene surface.

Fabrication of a Proof-of-Concept All-Solution Processable Sensor. Low-cost and scalable sensors are crucial for fabrication of wearable and PoC technologies.[22] In order to demonstrate the potential of graphene ink sensors for application in PoC testing, we fabricate a three-electrode, all-solution processable platform using a flexible polyimide substrate. Figure 6a provides a schematic overview of the proposed sensor with more details of the fabrication procedure provided in the Experimental Section. Briefly, a CO_2 laser printer is used to pattern a shadow mask in a sacrificial layer of

https://dx.doi.org/10.1021/acsami.0c21302
ACS Appl. Mater. Interfaces 2021, 13, 11185–11194

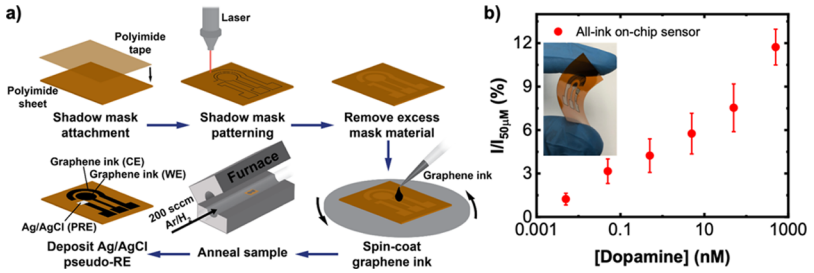

Figure 6. (a) Schematic of the fabrication process for the proof-of-concept all-solution processable sensor with CE and PREs made using graphene ink on a polyimide sheet. (b) The sensor response to DA in PBS measured using DPV. Inset—an optical image of a sensor fabricated on a polyimide substrate.

polyimide tape. The patterned polyimide is removed, and the graphene ink is then spin-coated. The sample is annealed at 300 °C for 30 min under, and a PRE is formed using bleach-treated Ag paste. The resulting sensor response is shown in Figure 6b. The response is similar to the samples tested using conventional counter and reference electrodes, as shown previously in Figure 3, thus demonstrating the graphene ink as a suitable platform for fabricating flexible, PoC biosensors.

CONCLUSIONS

We investigate a facile process for enhancing the sensitivity of commercial graphene ink toward DA oxidation in physiological pH and demonstrate its application as a low-cost sensing material. The effect of the annealing condition of spin-coated graphene ink on the surface chemistry and electrochemical properties is investigated. The optimal annealing condition for DA detection is found to be 300 °C for 30 min in a 3% H_2 + Ar environment. As determined by XPS analysis, this condition is found to have the largest levels of oxygen functionalities (in particular, C−OH) compared to the other three processing conditions. To understand how these results correlate with DA adsorption on graphene, we evaluate the non-faradaic charge accumulation of three amine-containing molecules, specifically DA, PEA, and PA. We find that $\pi-\pi$ interaction and hydroxyl groups of DA enhance its adsorption on graphene. Furthermore, in an effort to translate toward a PoC platform, a portable, all-solution processable sensor based on patterned graphene ink is developed.

Considering the wealth of active edge sites and defects in 2D material inks, they can serve as excellent candidates for developing low-cost and printable sensing devices/systems. Moreover, the use of 2D inks facilitates the formation of porous electrodes, which can offer additional "catalytic" enhancement over pristine, planar graphene films by modifying the mass transport properties of the electrode. This often manifests itself as a shift and/or splitting of the redox peak, as seen in this study. Further investigation into the effect of porosity in spin-coated, solution-processable electrodes on sensitivity toward the analyte is necessary. Additionally, studying the effect of other annealing environments and conditions (*e.g.*, other gases, dopants, *etc.*) on graphene and other 2D inks and their hybrids is warranted as it may offer a means to tune their response toward other clinically relevant biochemical analytes.

ASSOCIATED CONTENT

Supporting Information

The Supporting Information is available free of charge at https://pubs.acs.org/doi/10.1021/acsami.0c21302.

Optimization of graphene ink spin-coating conditions, morphology and electrochemical response of various spin-coating conditions, effect of hydrogen content on the DA oxidation peak, details of sheet resistance measurements and results for each annealing condition, effect of scan rate on DA peak currents using CV, Raman spectra and analysis for the various annealing conditions, and the XPS spectra and exemplary fitting scheme (PDF)

AUTHOR INFORMATION

Corresponding Author

Aida Ebrahimi − *Department of Electrical Engineering and Center for Atomically Thin Multifunctional Coatings, The Pennsylvania State University, University Park, Pennsylvania 16802, United States;* orcid.org/0000-0002-4013-7816; Email: sue66@psu.edu

Authors

Derrick Butler − *Department of Electrical Engineering and Center for Atomically Thin Multifunctional Coatings, The Pennsylvania State University, University Park, Pennsylvania 16802, United States;* orcid.org/0000-0003-3514-9326

David Moore − *Air Force Research Laboratory, Materials and Manufacturing Directorate, WPAFB, Dayton, Ohio 45433, United States*

Nicholas R. Glavin − *Air Force Research Laboratory, Materials and Manufacturing Directorate, WPAFB, Dayton, Ohio 45433, United States;* orcid.org/0000-0002-9447-7509

Joshua A. Robinson − *Center for Atomically Thin Multifunctional Coatings and Department of Materials Science and Engineering, The Pennsylvania State University, University Park, Pennsylvania 16802, United States*

Complete contact information is available at: https://pubs.acs.org/10.1021/acsami.0c21302

Notes

The authors declare no competing financial interest.

ACKNOWLEDGMENTS

D.B., J.A.R., and A.E. thank the Center for Atomically Thin Multifunctional Coatings (ATOMIC), a National Science Foundation I/UCRC program (award #1540018) for supporting this work. N.R.G. acknowledges support from the Air Force Office of Scientific Research under grant number FA9550-20RXCOR057. We also thank the Penn State Materials Research Institute (MRI) and Materials Characterization Lab (MCL), as well as the staff for their guidance and assistance with material and electrical characterization. The authors also appreciate Prof. M. Terrones and Dr. Y. Lei at Penn State

University for using their furnace to anneal polyimide substrates in a controlled environment.

REFERENCES

(1) Missale, C.; Nash, S. R.; Robinson, S. W.; Jaber, M.; Caron, M. G. Dopamine Receptors: From Structure to Function. *Physiol. Rev.* **1998**, *78*, 189−225.

(2) Wang, X.; Villar, V. A. M.; Armando, I.; Eisner, G. M.; Felder, R. A.; Jose, P. A. Dopamine, Kidney, and Hypertension: Studies in Dopamine Receptor Knockout Mice. *Pediatr. Nephrol.* **2008**, *23*, 2131−2146.

(3) Hornykiewicz, O. Dopamine (3-Hydroxytyramine) and Brain Function. *Pharmacol. Rev.* **1966**, *18*, 925−964.

(4) Da Prada, M.; Zürcher, G. Simultaneous Radioenzymatic Determination of Plasma and Tissue Adrenaline, Noradrenaline and Dopamine within the Femtomole Range. *Life Sci.* **1976**, *19*, 1161−1174.

(5) Robinson, D. L.; Venton, B. J.; Heien, M. L. A. V.; Wightman, R. M. Detecting Subsecond Dopamine Release with Fast-Scan Cyclic Voltammetry *in Vivo*. *Clin. Chem.* **2003**, *49*, 1763−1773.

(6) Sawka, A. M.; Jaeschke, R.; Singh, R. J.; Young, W. F. A Comparison of Biochemical Tests for Pheochromocytoma: Measurement of Fractionated Plasma Metanephrines Compared with the Combination of 24-Hour Urinary Metanephrines and Catecholamines. *J. Clin. Endocrinol. Metab.* **2003**, *88*, 553−558.

(7) Palanisamy, S.; Ku, S.; Chen, S.-M. Dopamine Sensor Based on a Glassy Carbon Electrode Modified with a Reduced Graphene Oxide and Palladium Nanoparticles Composite. *Microchim. Acta* **2013**, *180*, 1037−1042.

(8) Pandikumar, A.; Soon How, G. T.; See, T. P.; Omar, F. S.; Jayabal, S.; Kamali, K. Z.; Yusoff, N.; Jamil, A.; Ramaraj, R.; John, S. A.; Lim, H. N.; Huang, N. M. Graphene and Its Nanocomposite Material Based Electrochemical Sensor Platform for Dopamine. *RSC Adv.* **2014**, *4*, 63296−63323.

(9) Adams, R. N. Probing Brain Chemistry with Electroanalytical Techniques. *Anal. Chem.* **1976**, *48*, 1126A−1138A.

(10) Anithaa, A. C.; Lavanya, N.; Asokan, K.; Sekar, C. WO_3 Nanoparticles Based Direct Electrochemical Dopamine Sensor in the Presence of Ascorbic Acid. *Electrochim. Acta* **2015**, *167*, 294−302.

(11) Lei, Y.; Butler, D.; Lucking, M. C.; Zhang, F.; Xia, T.; Fujisawa, K.; Granzier-Nakajima, T.; Cruz-Silva, R.; Endo, M.; Terrones, H.; Terrones, M.; Ebrahimi, A. Single-Atom Doping of MoS_2 with Manganese Enables Ultrasensitive Detection of Dopamine: Experimental and Computational Approach. *Sci. Adv.* **2020**, *6*, No. eabc4250.

(12) Bard, A. J.; Faulkner, L. R. *Electrochemical Methods: Fundamentals and Applications*, 2nd ed.; John Wiley and Sons, Inc.: New York, 2001.

(13) Khudaish, E. A.; Al-Nofli, F.; Rather, J. A.; Al-Hinaai, M.; Laxman, K.; Kyaw, H. H.; Al-Harthy, S. Sensitive and Selective Dopamine Sensor Based on Novel Conjugated Polymer Decorated with Gold Nanoparticles. *J. Electroanal. Chem.* **2016**, *761*, 80−88.

(14) Novoselov, K. S.; Geim, A. K.; Morozov, S. V.; Jiang, D.; Zhang, Y.; Dubonos, S. V.; Grigorieva, I. V.; Firsov, A. A. Electric Field in Atomically Thin Carbon Films. *Science* **2004**, *306*, 666−669.

(15) Liao, K.-H.; Lin, Y.-S.; MacOsko, C. W.; Haynes, C. L. Cytotoxicity of Graphene Oxide and Graphene in Human Erythrocytes and Skin Fibroblasts. *ACS Appl. Mater. Interfaces* **2011**, *3*, 2607−2615.

(16) Sun, S.; Gao, L.; Liu, Y. Enhanced Dye-Sensitized Solar Cell Using Graphene- TiO_2 Photoanode Prepared by Heterogeneous Coagulation. *Appl. Phys. Lett.* **2010**, *96*, 083113.

(17) Prasai, D.; Tuberquia, J. C.; Harl, R. R.; Jennings, G. K.; Bolotin, K. I.; Bolotin, K. I. Graphene: Corrosion-Inhibiting Coating. *ACS Nano* **2012**, *6*, 1102−1108.

(18) Farell, M.; Self, A.; Guza, C.; Song, H.; Apollon, L.; Gomez, E. W.; Kumar, M. Lipid-Functionalized Graphene Loaded with HMnSOD for Selective Inhibition of Cancer Cells. *ACS Appl. Mater. Interfaces* **2020**, *12*, 12407−12416.

(19) Kang, X.; Wang, J.; Wu, H.; Liu, J.; Aksay, I. A.; Lin, Y. A Graphene-Based Electrochemical Sensor for Sensitive Detection of Paracetamol. *Talanta* **2010**, *81*, 754−759.

(20) Adhikari, B.-R.; Govindhan, M.; Chen, A. Sensitive Detection of Acetaminophen with Graphene-Based Electrochemical Sensor. *Electrochim. Acta* **2015**, *162*, 198−204.

(21) Sheng, Z.-H.; Zheng, X.-Q.; Xu, J.-Y.; Bao, W.-J.; Wang, F.-B.; Xia, X.-H. Electrochemical Sensor Based on Nitrogen Doped Graphene: Simultaneous Determination of Ascorbic Acid, Dopamine and Uric Acid. *Biosens. Bioelectron.* **2012**, *34*, 125−131.

(22) Bolotsky, A.; Butler, D.; Dong, C.; Gerace, K.; Glavin, N. R.; Muratore, C.; Robinson, J. A.; Ebrahimi, A. Two-Dimensional Materials in Biosensing and Healthcare: From In Vitro Diagnostics to Optogenetics and Beyond. *ACS Nano* **2019**, *13*, 9781−9810.

(23) Hu, S.; Huang, Q.; Lin, Y.; Wei, C.; Zhang, H.; Zhang, W.; Guo, Z.; Bao, X.; Shi, J.; Hao, A. Reduced Graphene Oxide-Carbon Dots Composite as an Enhanced Material for Electrochemical Determination of Dopamine. *Electrochim. Acta* **2014**, *130*, 805−809.

(24) Raj, M.; Gupta, P.; Goyal, R. N.; Shim, Y.-B. Graphene/Conducting Polymer Nano-Composite Loaded Screen Printed Carbon Sensor for Simultaneous Determination of Dopamine and 5-Hydroxytryptamine. *Sens. Actuators, B* **2017**, *239*, 993−1002.

(25) Punckt, C.; Pope, M. A.; Aksay, I. A. High Selectivity of Porous Graphene Electrodes Solely Due to Transport and Pore Depletion Effects. *J. Phys. Chem. C* **2014**, *118*, 22635−22642.

(26) Wang, W.; Wang, W.; Davis, J. J.; Luo, X. Ultrasensitive and Selective Voltammetric Aptasensor for Dopamine Based on a Conducting Polymer Nanocomposite Doped with Graphene Oxide. *Microchim. Acta* **2015**, *182*, 1123−1129.

(27) Liu, S.; Xing, X.; Yu, J.; Lian, W.; Li, J.; Cui, M.; Huang, J. A Novel Label-Free Electrochemical Aptasensor Based on Graphene-Polyaniline Composite Film for Dopamine Determination. *Biosens. Bioelectron.* **2012**, *36*, 186−191.

(28) Sharma, R.; Ragavan, K. V.; Thakur, M. S.; Raghavarao, K. S. M. S. Recent Advances in Nanoparticle Based Aptasensors for Food Contaminants. *Biosens. Bioelectron.* **2015**, *74*, 612−627.

(29) Li, S.-J.; He, J.-Z.; Zhang, M.-J.; Zhang, R.-X.; Lv, X.-L.; Li, S.-H.; Pang, H. Electrochemical Detection of Dopamine Using Water-Soluble Sulfonated Graphene. *Electrochim. Acta* **2013**, *102*, 58−65.

(30) Yang, L.; Liu, D.; Huang, J.; You, T. Simultaneous Determination of Dopamine, Ascorbic Acid and Uric Acid at Electrochemically Reduced Graphene Oxide Modified Electrode. *Sens. Actuators, B* **2014**, *193*, 166−172.

(31) Lin, J.; Peng, Z.; Liu, Y.; Ruiz-Zepeda, F.; Ye, R.; Samuel, E. L. G.; Yacaman, M. J.; Yakobson, B. I.; Tour, J. M. Laser-Induced Porous Graphene Films from Commercial Polymers. *Nat. Commun.* **2014**, *5*, 5714.

(32) Ye, R.; James, D. K.; Tour, J. M. Laser-Induced Graphene: From Discovery to Translation. *Adv. Mater.* **2019**, *31*, 1803621.

(33) Ge, L.; Hong, Q.; Li, H.; Liu, C.; Li, F. Direct-Laser-Writing of Metal Sulfide-Graphene Nanocomposite Photoelectrode toward Sensitive Photoelectrochemical Sensing. *Adv. Funct. Mater.* **2019**, *29*, 1904000.

(34) Ge, L.; Hong, Q.; Li, H.; Li, F. A Laser-Induced TiO2-Decorated Graphene Photoelectrode for Sensitive Photoelectrochemical Biosensing. *Chem. Commun.* **2019**, *55*, 4945−4948.

(35) Muralidharan, R.; Chandrashekhar, V.; Butler, D.; Ebrahimi, A. A Smartphone-Interfaced, Flexible Electrochemical Biosensor Based on Graphene Ink for Selective Detection of Dopamine. *IEEE Sens. J.* **2020**, *20*, 13204−13211.

(36) Bolotsky, A.; Muralidharan, R.; Butler, D.; Root, K.; Murray, W.; Liu, Z.; Ebrahimi, A. Organic Redox-Active Crystalline Layers for Reagent-Free Electrochemical Antibiotic Susceptibility Testing (ORACLE-AST). *Biosens. Bioelectron.* **2021**, *172*, 112615.

(37) Liu, Y. M.; Punckt, C.; Pope, M. A.; Gelperin, A.; Aksay, I. A. Electrochemical Sensing of Nitric Oxide with Functionalized Graphene Electrodes. *ACS Appl. Mater. Interfaces* **2013**, *5*, 12624−12630.

(38) Butler, D.; Robinson, J.; Ebrahimi, A. Tailoring Surface Chemistry of Graphene Ink for Highly-Sensitive Electrochemical Detection of Dopamine Down to 50 Picomolar. *ECS Meeting Abstracts*, 2020 https://ecs.confex.com/ecs/237/meetingapp.cgi/Paper/134335.

https://dx.doi.org/10.1021/acsami.0c21302
ACS Appl. Mater. Interfaces 2021, 13, 11185−11194

(39) Bath, B. D.; Michael, D. J.; Trafton, B. J.; Joseph, J. D.; Runnels, P. L.; Wightman, R. M. Subsecond Adsorption and Desorption of Dopamine at Carbon-Fiber Microelectrodes. *Anal. Chem.* **2000**, *72*, 5994−6002.
(40) Ren, H.; Kulkarni, D. D.; Kodiyath, R.; Xu, W.; Choi, I.; Tsukruk, V. V. Competitive Adsorption of Dopamine and Rhodamine 6G on the Surface of Graphene Oxide. *ACS Appl. Mater. Interfaces* **2014**, *6*, 2459−2470.
(41) Ortiz-Medina, J.; López-Urías, F.; Terrones, H.; Rodríguez-Macías, F. J.; Endo, M.; Terrones, M. Differential Response of Doped/Defective Graphene and Dopamine to Electric Fields: A Density Functional Theory Study. *J. Phys. Chem. C* **2015**, *119*, 13972−13978.
(42) Kovtun, A.; Jones, D.; Dell'Elce, S.; Treossi, E.; Liscio, A.; Palermo, V. Accurate Chemical Analysis of Oxygenated Graphene-Based Materials Using X-Ray Photoelectron Spectroscopy. *Carbon* **2019**, *143*, 268−275.
(43) Jakubowska, M. Signal Processing in Electrochemistry. *Electroanalysis* **2011**, *23*, 553−572.
(44) Secor, E. B.; Ahn, B. Y.; Gao, T. Z.; Lewis, J. A.; Hersam, M. C. Rapid and Versatile Photonic Annealing of Graphene Inks for Flexible Printed Electronics. *Adv. Mater.* **2015**, *27*, 6683−6688.
(45) Das, S. R.; Nian, Q.; Cargill, A. A.; Hondred, J. A.; Ding, S.; Saei, M.; Cheng, G. J.; Claussen, J. C. 3D Nanostructured Inkjet Printed Graphene: Via UV-Pulsed Laser Irradiation Enables Paper-Based Electronics and Electrochemical Devices. *Nanoscale* **2016**, *8*, 15870−15879.
(46) Das, S. R.; Srinivasan, S.; Stromberg, L. R.; He, Q.; Garland, N.; Straszheim, W. E.; Ajayan, P. M.; Balasubramanian, G.; Claussen, J. C. Superhydrophobic Inkjet Printed Flexible Graphene Circuits via Direct-Pulsed Laser Writing. *Nanoscale* **2017**, *9*, 19058−19065.
(47) Jiang, H.-B.; Zhang, Y.-L.; Han, D.-D.; Xia, H.; Feng, J.; Chen, Q.-D.; Hong, Z.-R.; Sun, H.-B. Bioinspired Fabrication of Superhydrophobic Graphene Films by Two-Beam Laser Interference. *Adv. Funct. Mater.* **2014**, *24*, 4595−4602.
(48) Silva, T. A.; Zanin, H.; Saito, E.; Medeiros, R. A.; Vicentini, F. C.; Corat, E. J.; Fatibello-Filho, O. Electrochemical Behaviour of Vertically Aligned Carbon Nanotubes and Graphene Oxide Nanocomposite as Electrode Material. *Electrochim. Acta* **2014**, *119*, 114−119.
(49) Hadi, M.; Rouhollahi, A. Simultaneous Electrochemical Sensing of Ascorbic Acid, Dopamine and Uric Acid at Anodized Nanocrystalline Graphite-like Pyrolytic Carbon Film Electrode. *Anal. Chim. Acta* **2012**, *721*, 55−60.
(50) Singh, D. P.; Herrera, C. E.; Singh, B.; Singh, S.; Singh, R. K.; Kumar, R. Graphene Oxide: An Efficient Material and Recent Approach for Biotechnological and Biomedical Applications. *Mater. Sci. Eng., C* **2018**, *86*, 173−197.
(51) Lee, J.; Kim, J.; Kim, S.; Min, D.-H. Biosensors Based on Graphene Oxide and Its Biomedical Application. *Adv. Drug Delivery Rev.* **2016**, *105*, 275−287.
(52) Wang, L.; Zhang, W.; Samavat, S.; Deganello, D.; Teng, K. S. Vertically Aligned Graphene Prepared by Photonic Annealing for Ultrasensitive Biosensors. *ACS Appl. Mater. Interfaces* **2020**, *12*, 35328−35336.
(53) Lai, H. L.; Pitt, K.; Craig, D. Q. M. Characterisation of the Thermal Properties of Ethylcellulose Using Differential Scanning and Quasi-Isothermal Calorimetric Approaches. *Int. J. Pharm.* **2010**, *386*, 178−184.
(54) Secor, E. B.; Prabhumirashi, P. L.; Puntambekar, K.; Geier, M. L.; Hersam, M. C. Inkjet Printing of High Conductivity, Flexible Graphene Patterns. *J. Phys. Chem. Lett.* **2013**, *4*, 1347−1351.
(55) Chen, P.; McCreery, R. L. Control of Electron Transfer Kinetics at Glassy Carbon Electrodes by Specific Surface Modification. *Anal. Chem.* **1996**, *68*, 3958−3965.
(56) Randviir, E. P.; Brownson, D. A. C.; Metters, J. P.; Kadara, R. O.; Banks, C. E. The Fabrication, Characterisation and Electrochemical Investigation of Screen-Printed Graphene Electrodes. *Phys. Chem. Chem. Phys.* **2014**, *16*, 4598−4611.
(57) (a) Valles, C.; David Nunez, J.; Benito, A. M.; Maser, W. K. Flexible conductive graphene paper obtained by direct and gentle annealing of graphene oxide paper. *Carbon* **2012**, *50* (3), 835−844. (b) Kobayashi, Y.; Fukui, K.-i.; Enoki, T.; Kusakabe, K.; Kaburagi, Y. Observation of zigzag and armchair edges of graphite using scanning tunneling microscopy and spectroscopy. *Phys. Rev. B: Condens. Matter Mater. Phys.* **2005**, *71*, 193406.
(58) Chang, Y.-C.; Sohn, H.-J. Electrochemical Impedance Analysis for Lithium Ion Intercalation into Graphitized Carbons. *J. Electrochem. Soc.* **2000**, *147*, 50−58.
(59) Ambrosi, A.; Bonanni, A.; Sofer, Z.; Cross, J. S.; Pumera, M. Electrochemistry at Chemically Modified Graphenes. *Chem.—Eur. J.* **2011**, *17*, 10763−10770.
(60) Boopathi, S.; Narayanan, T. N.; Senthil Kumar, S. Improved Heterogeneous Electron Transfer Kinetics of Fluorinated Graphene Derivatives. *Nanoscale* **2014**, *6*, 10140−10146.
(61) Luo, X.; Morrin, A.; Killard, A. J.; Smyth, M. R. Application of Nanoparticles in Electrochemical Sensors and Biosensors. *Electroanalysis* **2006**, *18*, 319−326.
(62) Streeter, I.; Wildgoose, G. G.; Shao, L.; Compton, R. G. Cyclic Voltammetry on Electrode Surfaces Covered with Porous Layers: An Analysis of Electron Transfer Kinetics at Single-Walled Carbon Nanotube Modified Electrodes. *Sens. Actuators, B* **2008**, *133*, 462−466.
(63) Punckt, C.; Pope, M. A.; Aksay, I. A. On the Electrochemical Response of Porous Functionalized Graphene Electrodes. *J. Phys. Chem. C* **2013**, *117*, 16076−16086.
(64) Brownson, D. A. C.; Varey, S. A.; Hussain, F.; Haigh, S. J.; Banks, C. E. Electrochemical Properties of CVD Grown Pristine Graphene: Monolayer- *vs.* Quasi-Graphene. *Nanoscale* **2014**, *6*, 1607−1621.
(65) Alwarappan, S.; Erdem, A.; Liu, C.; Li, C.-Z. Probing the Electrochemical Properties of Graphene Nanosheets for Biosensing Applications. *J. Phys. Chem. C* **2009**, *113*, 8853−8857.
(66) Pumera, M. Graphene-Based Nanomaterials and Their Electrochemistry. *Chem. Soc. Rev.* **2010**, *39*, 4146−4157.
(67) Dresselhaus, M. S.; Jorio, A.; Saito, R. Characterizing Graphene, Graphite, and Carbon Nanotubes by Raman Spectroscopy. *Annu. Rev. Condens. Matter Phys.* **2010**, *1*, 89−108.
(68) Wei, P.; Shen, J.; Wu, K.; Yang, N. Defect-Dependent Electrochemistry of Exfoliated Graphene Layers. *Carbon* **2019**, *154*, 125−131.
(69) Ross, M. A. Determination of Ascorbic Acid and Uric Acid in Plasma by High-Performance Liquid Chromatography. *J. Chromatogr. B: Biomed. Sci. Appl.* **1994**, *657*, 197−200.
(70) Fernández, A. C. R.; Castellani, N. J. Noncovalent Interactions between Dopamine and Regular and Defective Graphene. *ChemPhysChem* **2017**, *18*, 2065−2080.

https://dx.doi.org/10.1021/acsami.0c21302
ACS Appl. Mater. Interfaces 2021, 13, 11185−11194